Acta Cryst E CRYSTALLOGRAPHIC COMMUNICATIONS

ISSN 2056-9890

Crystal structure of $BaMnB_2O_5$ containing structurally isolated manganese oxide sheets

Elizabeth M. Maschmeyer,[a] Liurukara D. Sanjeewa[b] and Kulugammana G. S. Ranmohotti[a]*

[a]Division of Chemistry and Biological Sciences, Governors State University, 1 University Parkway, University Park, IL 60484-0975, USA, and [b]Department of Chemistry, Clemson University, Clemson, SC 29634-0973, USA. *Correspondence e-mail: kranmohotti@govst.edu

Received 24 June 2016
Accepted 12 August 2016

Edited by M. Weil, Vienna University of Technology, Austria

Keywords: crystal structure; pyroborates; interplanar angle; layered framework; bond-valence-sum calculations.

CCDC reference: 1499124

Supporting information: this article has supporting information at journals.iucr.org/e

In an attempt to search for mixed alkaline-earth and transition metal pyroborates, the title compound, barium manganese(II) pyroborate, has been synthesized by employing a flux method. The structure of $BaMnB_2O_5$ is composed of MnO_5 square pyramids that form Mn_2O_8 dimers by edge-sharing and of pyroborate units ($[B_2O_5]^{4-}$) that are composed of two corner-sharing trigonal–planar BO_3 units. These building blocks share corners to form $^2_\infty[MnB_2O_5]^{2-}$ layers extending parallel to (100). The Ba^{2+} cations reside in the gap between two manganese pyroborate slabs with a coordination number of nine. The title compound forms an interesting spiral framework propagating along the 2_1 screw axis. The structure is characterized by two alternating layers, which is relatively rare among known transition-metal-based pyroborate compounds.

1. Chemical context

Numerous borates with various crystal structures and compositions have been widely investigated over the last few decades (Heller *et al.*, 1986). Pyroborates containing the $(B_2O_5)^{4-}$ anion were first structurally characterized in 1950 (Berger, 1950). Pyroborates can be divided into two subclasses such as alkaline-earth-based pyroborates with general formula $A_2B_2O_5$ (A = alkaline earth metal) and transition-metal-based pyroborates with general formula $MM'B_2O_5$. If $M = M'$, the pyroborate is considered to be homo-metallic, otherwise it is hetero-metallic.

Alkaline-earth-based pyroborates adopt different structure types. During the investigation of the BaO/B_2O_3 system, Hubner revealed $Ba_2B_2O_5$ crystallizing in space group $P2/m$ (Hubner, 1969). The other alkaline-earth-based $A_2B_2O_5$ pyroborates (A = Mg, Ca, Sr) have been synthesized by high-temperature solid-state reactions. $Mg_2B_2O_5$ (Guo *et al.*, 1995*b*) crystallizes in space group $P2_1/c$. $Ca_2B_2O_5$ (Lin *et al.*, 1999*a*) and $Sr_2B_2O_5$ (Lin *et al.*, 1999*b*) are isotypic and crystallize in the same space group type as $Mg_2B_2O_5$ but have a different structure from the latter. Additionally, there exists a triclinic magnesium pyroborate ($P\overline{1}$; Guo *et al.*, 1995*a*). The existence of mixed alkaline-earth-based pyroborates ($AA'B_2O_5$) has been proven by the study of naturally occurring minerals. The crystal structures of two polymorphs of $CaMgB_2O_5$, kurchatovite and clinokurchatovite, have been originally determined in space group types $Pc2_1b$ (Yakubovich *et al.*, 1976) and $P2_1/c$ (Simonov *et al.*, 1980). However, the crystal structures of both minerals have been re-examined and refined in different space

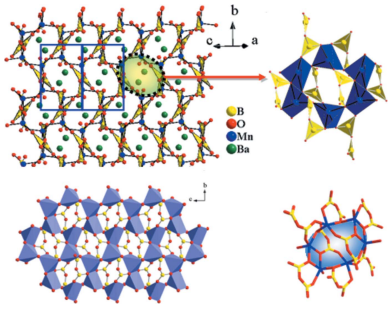

OPEN ACCESS

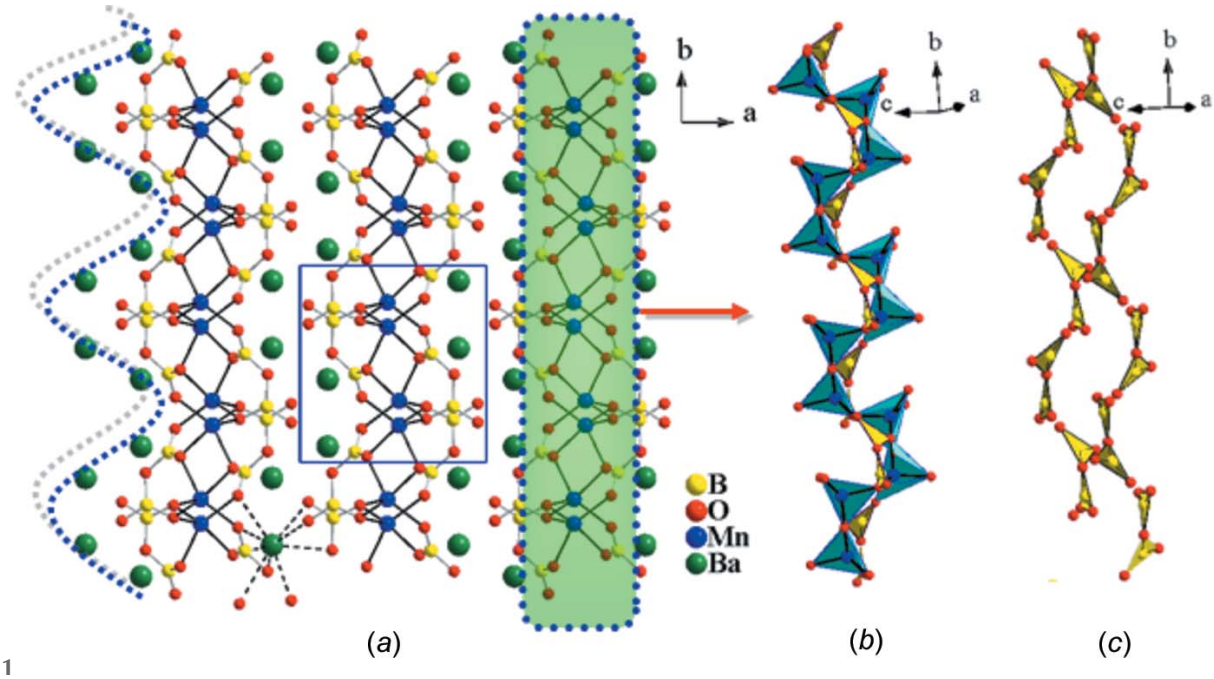

Figure 1
(*a*) Perspective view of the structure of $BaMnB_2O_5$ viewed along the *c* axis. The wavy and dotted line (left) indicates the zigzag arrays of Ba atoms. Only one Ba atom with bonds is drawn for clarity, demonstrating the function of Ba—O bonds with regard to holding neighboring $[MnB_2O_5]^{2-}$ slabs. (*b*) Polyhedral representation showing the $^2_\infty[MnB_2O_5]^{2-}$ spiral framework centered around the 2_1 screw axis of the unit cell. (*c*) Polyhedral representation showing the arrangement of isolated pyroborate units viewed approximately along the [101] direction.

group types (Callegari *et al.*, 2003). Based on these models, kurchatovite crystallizes in space group type *Pbca* whilst clinokurchatovite crystallizes in space group type $P2_1/c$.

Investigations of transition-metal-based homo-metallic pyroborates, $M_2B_2O_5$ have led to four compounds, namely $Mn_2B_2O_5$ (Sarrat *et al.*, 2005), $Co_2B_2O_5$ (Rowsell *et al.*, 2003), $Cd_2B_2O_5$ (Weil, 2003), and $Fe_2B_2O_5$ (Neumair & Huppertz, 2009). These phases crystallize isotypically with the triclinic form of $Mg_2B_2O_5$ (Guo *et al.*, 1995*a*). Efforts have been made to isolate transition-metal-based hetero-metallic phases, $MM'B_2O_5$. This has resulted in the synthesis of $MnCoB_2O_5$ and $MnMgB_2O_5$ (Utzolino & Bluhm, 1996), and $Ni_{1.5}Zn_{0.5}B_2O_5$ and $Co_{1.5}Zn_{0.5}B_2O_5$ (Busche & Bluhm, 1995). These structures are also isotypic with the triclinic form of $Mg_2B_2O_5$.

Investigations of the $BaO/CuO/B_2O_3$ phase diagram has resulted in the isolation of a non-centrosymmetric pyroborate, $BaCuB_2O_5$ (Smith & Keszler, 1997) with a unique structure type in space group type *C*2. As part of an effort to isolate new mixed alkaline earth and transition metal pyroborates, we have investigated the $BaO/MnO/B_2O_3$ phase diagram. In this study, we have grown single crystals of $BaMnB_2O_5$ and analyzed its crystal structure.

2. Structural commentary

The crystal structure of $BaMnB_2O_5$ defines a new structure type that can be described as being composed of manganese pyroborate slabs with composition $^2_\infty[MnB_2O_5]^{2-}$ that extend parallel to (100). Fig. 1*a* shows a perspective drawing of the $BaMnB_2O_5$ structure with the quasi-two-dimensional lattice characterized by $[MnB_2O_5]^{2-}$ slabs. The barium cations reside between the parallel slabs and maintain the interslab connectivity through coordination to nine oxygen atoms (Fig. 2*c*).

Two non-equivalent boron atoms are present in the structure; both are surrounded by three oxygen atoms to form almost regular trigonal–planar units. As depicted in Fig. 2*b*, the isolated $[B_2O_5]^{4-}$ pyroborate groups are composed of two corner-sharing trigonal–planar BO_3 units. In the reported pyroborate structures (Thompson *et al.*, 1991), the terminal BO_2 planes pivot about the torsion angles to afford deviations from coplanarity that can range from 0 to 76.8° where the B—O—B angle ranges from 112 to 180°. In $BaMnB_2O_5$, the pyroborate groups show closely related geometric features as previously noted (Thompson *et al.*, 1991), exhibiting a B—O—B angle of 125.1 (5)° whilst the dihedral angle between the two BO_3 units within the pyroborate group is 48.62 (8)°. The

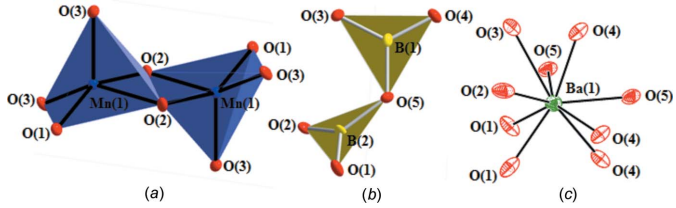

Figure 2
(*a*) Partial structure showing Mn_2O_8 dimers (polyhedral drawing). The apical oxygen, O3, in each MnO_5 square pyramid points in opposite directions. (*b*) Corner-sharing BO_3 groups forming a pyroborate unit. The BO_3 units within the pyroborate group are linked through a common O atom, O5. (*c*) The barium cation resides in a BaO_9 environment. Anisotropic displacement parameters are drawn at 95% probability.

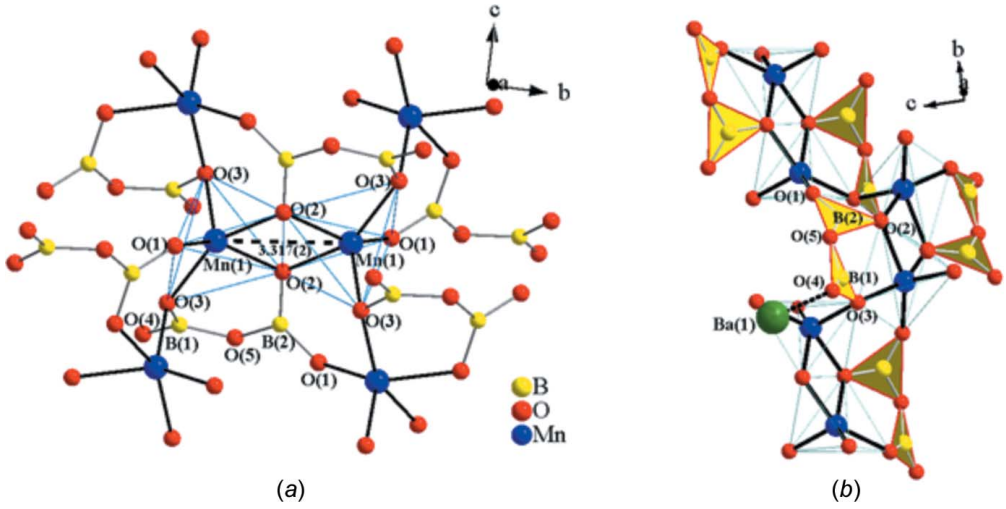

Figure 3
(*a*) The $Mn1O_5$ square pyramids (ball and stick drawing) share a common edge, O2—O2, forming an Mn_2O_8 unit. (*b*) The $B2O_3$ unit (polyhedral drawing), shares two corners with neighboring MnO_5 square pyramids (ball and stick drawing) through O1 and O2. The only unshared oxygen, O4, of the pyroborate group forms a bond with a Ba atom.

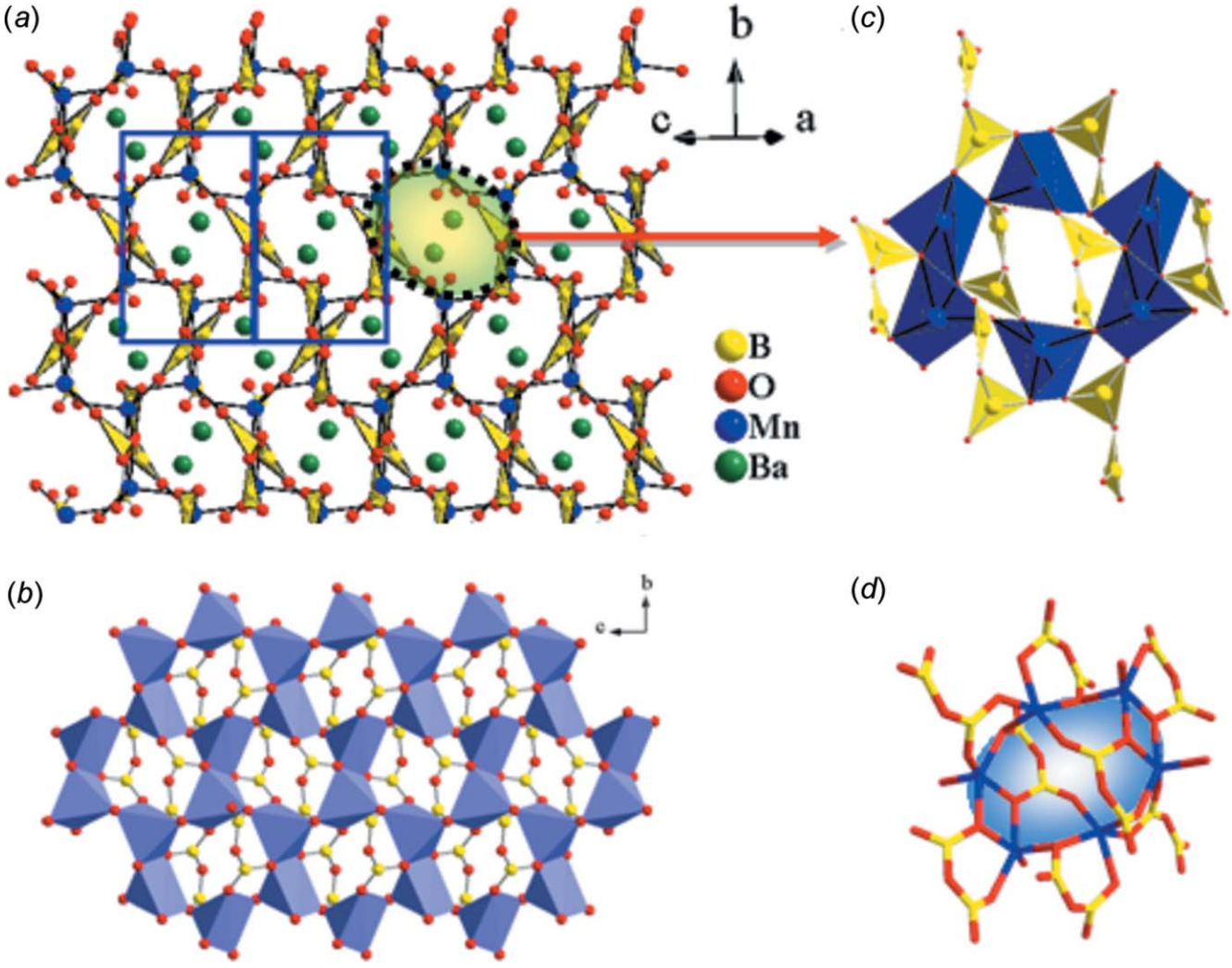

Figure 4
(*a*) Extended structure of $BaMnB_2O_5$ viewed approximately along the [101] direction. The connectivity of the barium atoms is not shown for clarity. (*b*) Partial structure of $[MnB_2O_5]^{2-}$ slab viewed along [100] where the polyhedral drawing represents MnO_5 square pyramids and B_2O_5 units are represented by ball-and-stick drawing. (*c*) Edge-sharing and corner-sharing MnO_5 units corner-share with B_2O_5 pyroborate groups (polyhedral drawing) to create a cage. (*d*) Stick drawing of one cage with empty space in the middle.

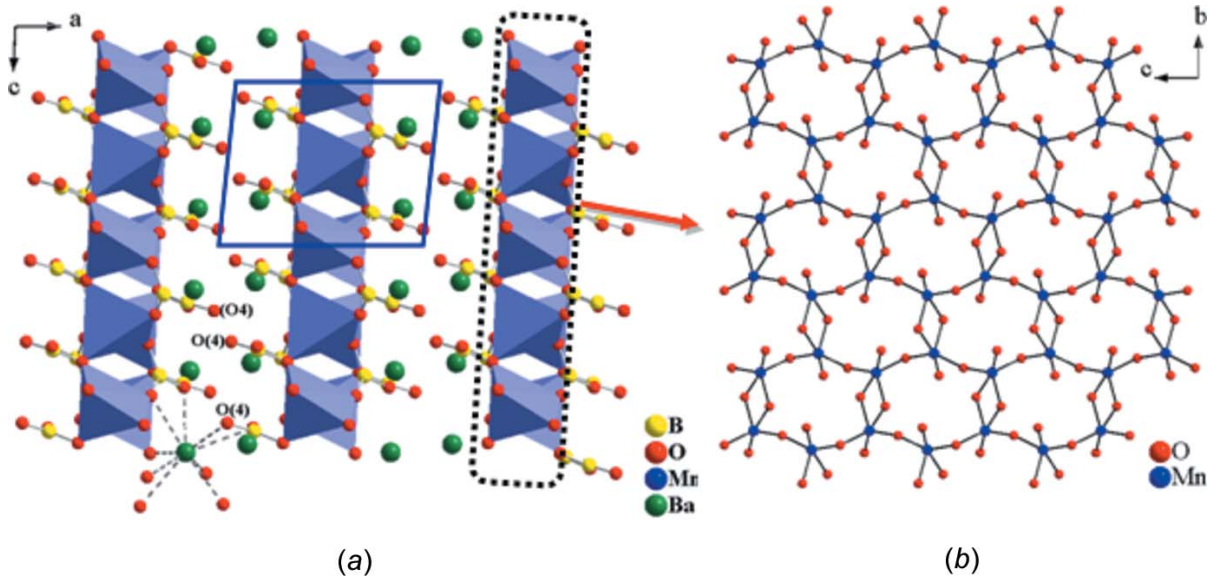

Figure 5
(*a*) Layered $BaMnB_2O_5$ shown by polyhedral and ball-and-stick drawing viewed along the [010] direction. (*b*) Ball-and-stick drawing of a portion of the manganese oxide network formed by interconnected Mn_2O_8 dimers by corner sharing.

asymmetry of the bond lengths in the B_2O_5 group is indicated by slightly varied bond lengths of terminal and bridging B—O bonds. The bridging B—O bond lengths are slightly longer [B1—O5: 1.423 (7); B2—O5: 1.432 (7) Å] than the terminal B—O bond lengths [range 1.332 (8)–1.384 (7) Å]. Notwithstanding, the average B—O bond length (1.380 Å) in the title compound is very close to the corresponding average B—O bond length in BO_3 groups in previously reported borates (1.370 Å; Zobetz, 1982). Fig. 1*c* shows the arrangement of isolated pyroborate units, appearing as two parallel pseudo-one-dimensional chains spiraling around the 2_1 axis.

There is one crystallographically independent Mn atom which is coordinated by five oxygen atoms to form a square pyramid with four longer equatorial Mn—O bonds and one short apical Mn—O bond. Fig. 2*a* shows two $Mn1O_5$ square pyramids sharing a common edge, O2—O2($-x+1, -y, -z$), to form an Mn_2O_8 unit. As shown in Fig. 3*a*, Mn atoms are connected to each other *via* oxygen atoms with a Mn1···Mn1 separation of 3.317 (2) Å and an Mn1—O2—Mn1 angle of 101.23 (16)°. The neighboring Mn_2O_8 dimers share vertices through oxygen atom O3. The oxygen atom O1 in the Mn_2O_8 dimer is only corner-shared by the pyroborate group. The only unshared oxygen, O4, of the pyroborate group is pointing into the free space towards the neighboring slabs to form a bond with the barium atom. As shown in Fig. 3*b*, with respect to the pyroborate group, the $B2O_3$ unit shares two corners with neighboring MnO_5 square pyramids through O1 and O2 while the $B1O_3$ unit corner-shares a common oxygen atom, O3, with two other MnO_5 square pyramids. This arrangement facilitates the observed curvature which is necessary for the spiral framework found in the extended lattice (Fig. 1*b*). The unique arrangement of B_2O_5 groups around the 2_1 screw axis provides an essential element allowing the spiral chain to propagate along the *b* axis. It is well known that the interplanar angle of the B_2O_5 group is primarily dictated by packing effects and the nature of the associated cations in the given structure (Thompson *et al.*, 1991). In addition to that, as previously noted, the greater deviations from coplanarity are observed in the arrangement of the B_2O_5 groups due to variation of the sizes of alkali metals in alkali metal Nb and Ta oxide pyroborates (Akella & Keszler, 1995). Accordingly, the interplanar angle of the B_2O_5 group is likely to be determined by the associate coordination environment of the barium cations in the title compound. It should be noted that the connectivity of the Mn_2O_8 and B_2O_5 structure units would result in a 'dangling' framework unless it can be tightly held together by external bonds. The Ba^{2+} cations, in this case, reside in the spiral framework arranging in zigzag fashion to support and maintain the distance between neighboring $[MnB_2O_5]^{2-}$ slabs. Coincidentally, this wavy arrangement is critical for the spiral chain to propagate along the *b* axis. The flexible $[MnB_2O_5]^{2-}$ framework revolves around Ba^{2+} cations, suggesting a template-like behavior.

The MnO_5 units adopt bond lengths normally observed in the Mn^{II} borates. The Mn^{2+}—O bond lengths range from 2.082 (4) to 2.151 (4) Å, comparable with 2.10 Å, the sum of the Shannon crystal radii (Shannon, 1976) for a five coordinated Mn^{2+} (0.89 Å) and two-coordinated O^{2-} (1.21 Å). The bond-valence-sum (BVS) calculations (Brese & O'Keeffe, 1991) for $BaMnB_2O_5$ give a valence unit (v.u.) of 2.03 for the Mn^{2+} cation. Based on parameters for B^{3+}—O, bond-valence sums of 2.95 for $B1^{3+}$ and 2.95 for $B2^{3+}$ were calculated. The Ba—O bond lengths are quite diverse, ranging from 2.707 (4) to 2.958 (4) Å. The average Ba—O bond length, 2.83 Å, however matches closely with 2.82 Å, the sum of the Shannon crystal radii for a nine coordinated Ba^{2+} (1.61 Å) and two-coordinated O^{2-} (1.21 Å). The BVS calculation for Ba^{2+} results in 2.08 v.u.

One of the interesting features of the title compound is that the structure can be alternatively viewed as a 'porous'

framework as shown in Fig. 4*a*. The B_2O_5 units together with interconnected Mn_2O_8 dimers extend along the *b* axis in a standing wave fashion, creating oval shape windows which also arrange in a zigzag fashion along the same direction. It is intriguing to notice that the two B_2O_5 groups along with the two Mn_2O_8 dimers and two MnO_5 square pyramids create an empty cage (Fig. 4*c*,*d*). The polyhedral and ball-and-stick drawing (Fig. 4*b*) clearly shows the three-dimensional framework bearing large cavities. This unusual structural arrangement is conceivably attributed to the limitation of the size of the pyroborate unit that simultaneously tends to interconnect with barium cations and neighboring Mn_2O_8 dimers in a corner-shared fashion (Fig. 3*b*). As shown in Fig. 5*a*, the layered nature of the title compound is characterized by parallel $[MnB_2O_5]^{2-}$ slabs outlined by a dotted rectangle viewed along [010]. Fig. 5*b* shows the ball-and-stick drawing of a portion of the layered manganese oxide network. Each Mn_2O_8 dimer shares vertices with four other MnO_5 square pyramids through oxygen atoms to form these sheets. Within the extended Mn—O sheet, the MnO_5 square pyramids which share edges are separated from each other by 3.317 (2) Å (Mn1···Mn1 distance) whereas those which share corners are separated by 3.435 (1) Å. The distance between the Mn atoms of the adjacent sheets is 8.287 (2) Å. Given the description of the local configuration of the manganese oxide polyhedra, their connectivity along the sheet, and the structural isolation of neighboring Mn—O sheets from each other, one would suspect that the title compound offers opportunities for the study of spin exchange in a confined Mn—O lattice. In theory, a periodic array of well-defined transition metal oxide lattices could provide a useful model for experimental and theoretical developments of magnetic and electronic interactions in transition metal oxides because of their simplified structures (Snyder *et al.*, 2001).

The structure of $BaMnB_2O_5$ is somewhat related to that of triclinic $M_2B_2O_5$ (*M* = Mn, Sarrat *et al.*, 2005; Fe, Neumair & Huppertz, 2009; Co, Rowsell *et al.*, 2003) phases. The structures of $M_2B_2O_5$ (*M* = Mn, Fe, Co) phases are based on structurally isolated $[M_4O_{18}]$ tetramers, composed of four octahedra linked by three shared edges, connected through sharing four O—O edges, into ribbons extending along (001) while the boron atoms hold the ribbons together forming B_2O_5 groups. These extended ribbons are parallel to each other and therefore these $M_2B_2O_5$ phases have a quasi-one-dimensional structure in contrast to the two-dimensional Mn—O lattice in the title compound. Magnetic properties have been widely studied for $Co_2B_2O_5$ (Kawano *et al.*, 2010), $Fe_2B_2O_5$ (Kawano *et al.*, 2009), and $Mn_2B_2O_5$ (Fernandes *et al.*, 2003) to understand the low-dimensional interactions derived from the ribbon-like substructures in these compounds. The spin configuration based on the electron-density distribution has been proposed (Sarrat *et al.*, 2005) for $Mn_2B_2O_5$ in which the distance between manganese atoms of adjacent ribbons are 4.526–6.272 Å and electron-density distributions were indicated in the regions between the ribbons. According to their model, all coplanar ribbons of $Mn_2B_2O_5$ are ferromagnetic; their antiferromagnetic behavior is derived from antiparallel magnetic orientations between adjacent ribbons. In the title compound, the distance between manganese atoms within the sheets and adjacent sheets are 3.317 (2)–3.435 (1) Å and 8.287 (2) Å, respectively. It is important to note that the Ba^{2+} cations reside in the gap between the two Mn—O sheets. This, together with the greater separation between manganese atoms of adjacent sheets, leads us to believe that magnetic interactions that occur between Mn—O sheets can be extremely weak and the dominant magnetic exchange should be between Mn^{2+} ions within the Mn—O sheet. Judging from the interesting magnetic properties reported for $M_2B_2O_5$ (*M* = Mn, Fe, Co) compounds, we expect interesting magnetic phenomena from a systematic investigation of the magnetic susceptibility of $BaMnB_2O_5$.

Table 1
Experimental details.

Crystal data	
Chemical formula	$BaMnB_2O_5$
M_r	293.90
Crystal system, space group	Monoclinic, $P2_1/c$
Temperature (K)	300
a, *b*, *c* (Å)	8.2868 (17), 8.6570 (17), 6.5263 (13)
β (°)	92.87 (3)
V (Å^3)	467.60 (16)
Z	4
Radiation type	Mo $K\alpha$
μ (mm^{-1})	10.99
Crystal size (mm)	0.17 × 0.05 × 0.02
Data collection	
Diffractometer	Rigaku AFC8S
Absorption correction	Multi-scan (*REQAB*; Rigaku, 1998)
T_{min}, T_{max}	0.518, 0.808
No. of measured, independent and observed [$I > 2\sigma(I)$] reflections	3807, 830, 777
R_{int}	0.052
(sin $\theta/\lambda)_{max}$ (Å^{-1})	0.598
Refinement	
$R[F^2 > 2\sigma(F^2)]$, $wR(F^2)$, S	0.025, 0.056, 1.10
No. of reflections	830
No. of parameters	83
$\Delta\rho_{max}$, $\Delta\rho_{min}$ (e Å^{-3})	0.82, −0.98

Computer programs: *CrystalClear* (Rigaku, 2006), *SHELXT* (Sheldrick, 2015*a*), *SHELXL2014* (Sheldrick, 2015*b*), *DIAMOND* (Brandenburg, 1999) and *publCIF* (Westrip, 2010).

3. Synthesis and crystallization

Light pink crystals of $BaMnB_2O_5$ were grown by employing a CsCl/RbCl flux in a fused silica ampoule under vacuum. MnO (2.74 mmol, 99.999+%, Alfa), BaO (1.37 mmol, 99.99+%, Aldrich) and B_2O_3 (1.37 mmol, 99.98+%, Aldrich) were mixed and ground with the flux (1:3 by weight) in a nitrogen-blanketed drybox. The resulting mixture was heated to 818 K at 1 K min^{-1}, isothermed for two days, heated to 1023 K at 1 K min^{-1}, isothermed for four days, then slowly cooled to 673 K at 0.1 K min^{-1} followed by furnace-cooling to room temperature. Prismatic crystals of $BaMnB_2O_5$ were retrieved upon washing off the solidified melt with deionized water.

4. Refinement

Crystal data, data collection and structure refinement details are summarized in Table 1. The final Fourier difference synthesis showed the maximum residual electron density in the difference Fourier map, 0.82 e $Å^{-3}$, located at 1.19 Å from Ba1 and the minimum, −0.98 e^{-} $Å^{-3}$, at 0.92 Å from Ba1.

Acknowledgements

The Division of Science at Governors State University is gratefully acknowledged for the continuous support. Special thanks are due to Dr Julien P. A. Makongo for his X-ray crystallography expertise.

References

Akella, A. & Keszler, D. A. (1995). *J. Solid State Chem.* **120**, 74–79.
Berger, S. V. (1950). *Acta Chem. Scand.* **4**, 1054–1065.
Brandenburg, K. (1999). *DIAMOND*. Crystal Impact GbR, Bonn, Germany.
Brese, N. E. & O'Keeffe, M. (1991). *Acta Cryst.* B**47**, 192–197.
Busche, S. & Bluhm, K. (1995). *Z. Naturforsch. Teil B*, **50**, 1445–1449.
Callegari, A., Mazzi, F. & Tadini, C. (2003). *Eur. J. Miner.* **15**, 277–282.
Fernandes, J. C., Sarrat, F. S., Guimarães, R. B., Freitas, R. S., Continentino, M. A., Doriguetto, A. C., Mascarenhas, Y. P., Ellena, J., Castellano, E. E., Tholence, J. L., Dumas, J. & Ghivelder, L. (2003). *Phys. Rev. B*, **67**, 104413-1-104413-7.
Guo, G.-C., Cheng, W.-D., Chen, J.-T., Huang, J.-S. & Zhang, Q.-E. (1995*a*). *Acta Cryst.* C**51**, 351–353.
Guo, G.-C., Cheng, W.-D., Chen, J.-T., Zhuang, H.-H., Huang, J.-S. & Zhang, Q.-E. (1995*b*). *Acta Cryst.* C**51**, 2469–2471.
Heller, G. (1986). *Top. Curr. Chem*. **131**, 39-98.
Hubner, K. H. (1969). *Neues Jahrb. Mineral. Monatsh.* pp. 335–343.
Kawano, T., Morito, H., Yamada, T., Onuma, T., Chichibu, S. F. & Yamane, H. (2009). *J. Solid State Chem.* **182**, 2004–2009.
Kawano, T., Morito, H. & Yamane, H. (2010). *Solid State Sci.* **12**, 1419–1421.
Lin, Q.-S., Cheng, W.-D., Chen, J.-T. & Huang, J.-S. (1999*a*). *Acta Cryst.* C**55**, 4–6.
Lin, Q.-S., Cheng, W.-D., Chen, J.-T. & Huang, J.-S. (1999*b*). *J. Solid State Chem.* **144**, 30–34.
Neumair, S. C. & Huppertz, H. (2009). *Z. Naturforsch. Teil B*, **64**, 491–498.
Rigaku (1998). *REQAB*. Rigaku Corporation, Tokyo, Japan.
Rigaku (2006). *CrystalClear*. Rigaku Corporation, Tokyo, Japan.
Rowsell, J. L. C., Taylor, N. J. & Nazar, L. F. (2003). *J. Solid State Chem.* **174**, 189–197.
Sarrat, F. S., Guimarães, R. B., Continentino, M. A., Fernandes, J. C., Doriguetto, A. C. & Ellena, J. (2005). *Phys. Rev. B*, **71**, 224413-1-224413-6.
Shannon, R. D. (1976). *Acta Cryst.* A**32**, 751–767.
Sheldrick, G. M. (2015*a*). *Acta Cryst.* A**71**, 3–8.
Sheldrick, G. M. (2015*b*). *Acta Cryst.* C**71**, 3–8.
Simonov, M. A., Egorov-Tismenko, Yu. K., Yamnova, N. A., Belokoneva, E. L. & Belov, N. V. (1980). *Dokl. Akad. Nauk SSSR*, **251**, 1125–1128.
Smith, R. W. & Keszler, D. A. (1997). *J. Solid State Chem.* **129**, 184–188.
Snyder, J., Slusky, J. S., Cava, R. J. & Schiffer, P. (2001). *Nature*, **413**, 48–51.
Thompson, P. D., Huang, J., Smith, R. W. & Keszler, D. A. (1991). *J. Solid State Chem.* **95**, 126–135.
Utzolino, A. & Bluhm, K. (1996). *Z. Naturforsch. Teil B*, **51**, 912–916.
Weil, M. (2003). *Acta Cryst.* E**59**, i95–i97.
Westrip, S. P. (2010). *J. Appl. Cryst.* **43**, 920–925.
Yakubovich, O. V., Yamnova, N. A., Shchedrin, B. M., Simonov, M. A. & Belov, N. V. (1976). *Dokl. Akad. Nauk SSSR*, **228**, 842–845.
Zobetz, E. (1982). *Z. Kristallogr.* **160**, 81–92.

supporting information

Acta Cryst. (2016). E**72**, 1315-1320 [doi:10.1107/S2056989016013074]

Crystal structure of $BaMnB_2O_5$ containing structurally isolated manganese oxide sheets

Elizabeth M. Maschmeyer, Liurukara D. Sanjeewa and Kulugammana G. S. Ranmohotti

Computing details

Data collection: *CrystalClear* (Rigaku, 2006); cell refinement: *CrystalClear* (Rigaku, 2006); data reduction: *CrystalClear* (Rigaku, 2006); program(s) used to solve structure: SHELXT (Sheldrick, 2015a); program(s) used to refine structure: *SHELXL2014* (Sheldrick, 2015b); molecular graphics: *DIAMOND* (Brandenburg, 1999); software used to prepare material for publication: *publCIF* (Westrip, 2010).

Barium manganese(II) pyroborate

Crystal data

$BaMnB_2O_5$
M_r = 293.90
Monoclinic, $P2_1/c$
a = 8.2868 (17) Å
b = 8.6570 (17) Å
c = 6.5263 (13) Å
β = 92.87 (3)°
V = 467.60 (16) Å^3
Z = 4
$F(000)$ = 524
D_x = 4.175 Mg m^{-3}
Mo $K\alpha$ radiation, λ = 0.71073 Å
Cell parameters from 3139 reflections
θ = 3.1–29.6°
μ = 10.99 mm^{-1}
T = 300 K
Prismatic, pink
0.17 × 0.05 × 0.02 mm

Data collection

Rigaku AFC8S diffractometer
Radiation source: fine-focus sealed tube
ω scans
Absorption correction: multi-scan (*REQAB*; Rigaku, 1998)
T_{min} = 0.518, T_{max} = 0.808
3807 measured reflections
830 independent reflections
777 reflections with $I > 2\sigma(I)$
R_{int} = 0.052
θ_{max} = 25.2°, θ_{min} = 3.4°
h = −9→9
k = −10→10
l = −7→7
1 standard reflections every 1 reflections

Refinement

Refinement on F^2
Least-squares matrix: full
$R[F^2 > 2\sigma(F^2)]$ = 0.025
$wR(F^2)$ = 0.056
S = 1.10
830 reflections
83 parameters
0 restraints
$w = 1/[\sigma^2(F_o^2) + (0.0315P)^2]$ where $P = (F_o^2 + 2F_c^2)/3$
$(\Delta/\sigma)_{max}$ = 0.005
$\Delta\rho_{max}$ = 0.82 e Å^{-3}
$\Delta\rho_{min}$ = −0.98 e Å^{-3}
Extinction correction: SHELXL2014 (Sheldrick, 2015b), $Fc^*=kFc[1+0.001xFc^2\lambda^3/\sin(2\theta)]^{-1/4}$
Extinction coefficient: 0.0061 (7)

Special details

Geometry. All esds (except the esd in the dihedral angle between two l.s. planes) are estimated using the full covariance matrix. The cell esds are taken into account individually in the estimation of esds in distances, angles and torsion angles; correlations between esds in cell parameters are only used when they are defined by crystal symmetry. An approximate (isotropic) treatment of cell esds is used for estimating esds involving l.s. planes.

Fractional atomic coordinates and isotropic or equivalent isotropic displacement parameters (Å²)

	x	*y*	*z*	U_{iso}*/U_{eq}
Ba1	0.14891 (4)	0.07969 (4)	0.22488 (5)	0.00932 (16)
Mn1	0.53148 (10)	0.18805 (10)	0.02929 (12)	0.0087 (2)
B1	0.1784 (8)	−0.2828 (7)	0.1447 (10)	0.0100 (13)
B2	0.2960 (8)	0.4492 (7)	0.1980 (10)	0.0115 (13)
O1	0.3314 (5)	0.3308 (4)	0.0723 (6)	0.0133 (9)
O2	0.3587 (5)	0.0300 (4)	−0.1080 (6)	0.0126 (9)
O3	0.3228 (5)	−0.2185 (4)	0.2184 (6)	0.0106 (8)
O4	0.0457 (5)	−0.2018 (4)	0.0939 (6)	0.0110 (8)
O5	−0.1725 (5)	0.0536 (4)	0.3763 (6)	0.0109 (8)

Atomic displacement parameters (Å²)

	U^{11}	U^{22}	U^{33}	U^{12}	U^{13}	U^{23}
Ba1	0.0103 (2)	0.0088 (2)	0.0088 (2)	0.00002 (12)	−0.00031 (13)	−0.00026 (13)
Mn1	0.0094 (5)	0.0080 (4)	0.0086 (5)	0.0000 (3)	−0.0006 (3)	−0.0001 (3)
B1	0.006 (3)	0.013 (3)	0.011 (3)	−0.002 (3)	0.000 (2)	0.002 (3)
B2	0.010 (3)	0.011 (3)	0.014 (3)	0.005 (3)	0.000 (3)	−0.003 (3)
O1	0.012 (2)	0.015 (2)	0.013 (2)	0.0056 (17)	−0.0030 (17)	−0.0054 (17)
O2	0.017 (2)	0.0073 (18)	0.012 (2)	−0.0008 (16)	−0.0055 (17)	−0.0004 (16)
O3	0.0108 (19)	0.0109 (19)	0.010 (2)	−0.0023 (16)	−0.0002 (16)	0.0011 (16)
O4	0.012 (2)	0.009 (2)	0.012 (2)	0.0033 (16)	0.0004 (16)	−0.0018 (16)
O5	0.013 (2)	0.0075 (19)	0.012 (2)	0.0010 (16)	−0.0036 (16)	0.0006 (16)

Geometric parameters (Å, º)

Ba1—O4	2.707 (4)	Mn1—O1	2.098 (4)
Ba1—O1^{i}	2.772 (4)	Mn1—O2	2.144 (4)
Ba1—O4^{ii}	2.777 (4)	Mn1—O2^{v}	2.147 (4)
Ba1—O4^{iii}	2.787 (4)	Mn1—O3^{vi}	2.151 (4)
Ba1—O5^{iv}	2.845 (4)	B1—O4	1.332 (8)
Ba1—O1	2.855 (4)	B1—O3	1.384 (7)
Ba1—O2	2.882 (4)	B1—O5^{vii}	1.423 (7)
Ba1—O5	2.896 (4)	B2—O1	1.354 (7)
Ba1—O3	2.958 (4)	B2—O2^{i}	1.357 (8)
Mn1—O3^{v}	2.082 (4)	B2—O5^{iii}	1.432 (7)
O4—Ba1—O1^{i}	131.36 (11)	O1—Mn1—O2^{v}	144.52 (16)
O4—Ba1—O4^{ii}	86.77 (11)	O2—Mn1—O2^{v}	78.77 (16)
O1^{i}—Ba1—O4^{ii}	141.16 (11)	O3^{v}—Mn1—O3^{vi}	102.81 (15)

O4—Ba1—O4^{iii}	124.37 (5)	O1—Mn1—O3^{vi}	95.36 (15)
O1^{i}—Ba1—O4^{iii}	76.50 (12)	O2—Mn1—O3^{vi}	153.85 (15)
O4^{ii}—Ba1—O4^{iii}	74.51 (8)	O2^{v}—Mn1—O3^{vi}	86.12 (14)
O4—Ba1—O5^{iv}	85.98 (11)	O1—B2—O2^{i}	125.6 (5)
O1^{i}—Ba1—O5^{iv}	49.87 (11)	O1—B2—O5^{iii}	116.5 (5)
O4^{ii}—Ba1—O5^{iv}	148.29 (11)	O2^{i}—B2—O5^{iii}	117.8 (5)
O4^{iii}—Ba1—O5^{iv}	84.37 (11)	B2—O1—Mn1	136.3 (4)
O4—Ba1—O1	137.70 (12)	B2—O1—Ba1^{viii}	99.1 (3)
O1^{i}—Ba1—O1	78.21 (9)	Mn1—O1—Ba1^{viii}	117.24 (16)
O4^{ii}—Ba1—O1	75.33 (12)	B2—O1—Ba1	103.3 (3)
O4^{iii}—Ba1—O1	87.65 (11)	Mn1—O1—Ba1	91.97 (13)
O5^{iv}—Ba1—O1	127.91 (11)	Ba1^{viii}—O1—Ba1	102.80 (13)
O4—Ba1—O2	79.67 (11)	B2^{viii}—O2—Mn1	121.5 (4)
O1^{i}—Ba1—O2	109.48 (11)	B2^{viii}—O2—Mn1^{v}	118.6 (4)
O4^{ii}—Ba1—O2	80.88 (11)	Mn1—O2—Mn1^{v}	101.23 (16)
O4^{iii}—Ba1—O2	143.59 (11)	B2^{viii}—O2—Ba1	117.8 (4)
O5^{iv}—Ba1—O2	127.79 (11)	Mn1—O2—Ba1	90.29 (13)
O1—Ba1—O2	60.05 (11)	Mn1^{v}—O2—Ba1	102.44 (14)
O4—Ba1—O5	75.88 (11)	B1—O3—Mn1^{v}	107.8 (4)
O1^{i}—Ba1—O5	102.48 (11)	B1—O3—Mn1^{ix}	123.9 (3)
O4^{ii}—Ba1—O5	77.04 (12)	Mn1^{v}—O3—Mn1^{ix}	108.48 (17)
O4^{iii}—Ba1—O5	49.20 (11)	B1—O3—Ba1	86.7 (3)
O5^{iv}—Ba1—O5	71.25 (13)	Mn1^{v}—O3—Ba1	101.68 (14)
O1—Ba1—O5	133.67 (10)	Mn1^{ix}—O3—Ba1	124.92 (15)
O2—Ba1—O5	147.72 (11)	B1—O4—Ba1	98.7 (3)
O4—Ba1—O3	49.93 (11)	B1—O4—Ba1^{ii}	145.9 (4)
O1^{i}—Ba1—O3	90.55 (11)	Ba1—O4—Ba1^{ii}	93.23 (11)
O4^{ii}—Ba1—O3	125.91 (11)	B1—O4—Ba1^{vii}	91.4 (3)
O4^{iii}—Ba1—O3	153.01 (10)	Ba1—O4—Ba1^{vii}	131.11 (15)
O5^{iv}—Ba1—O3	69.38 (11)	Ba1^{ii}—O4—Ba1^{vii}	104.46 (13)
O1—Ba1—O3	113.11 (11)	B1^{iii}—O5—B2^{vii}	125.1 (5)
O2—Ba1—O3	63.01 (10)	B1^{iii}—O5—Ba1^{iv}	119.5 (3)
O5—Ba1—O3	113.20 (11)	B2^{vii}—O5—Ba1^{iv}	93.9 (3)
O3^{v}—Mn1—O1	121.48 (15)	B1^{iii}—O5—Ba1	85.3 (3)
O3^{v}—Mn1—O2	99.07 (15)	B2^{vii}—O5—Ba1	126.0 (3)
O1—Mn1—O2	85.17 (16)	Ba1^{iv}—O5—Ba1	108.75 (13)
O3^{v}—Mn1—O2^{v}	92.39 (15)		

Symmetry codes: (i) x, $-y+1/2$, $z+1/2$; (ii) $-x$, $-y$, $-z$; (iii) $-x$, $y+1/2$, $-z+1/2$; (iv) $-x$, $-y$, $-z+1$; (v) $-x+1$, $-y$, $-z$; (vi) $-x+1$, $y+1/2$, $-z+1/2$; (vii) $-x$, $y-1/2$, $-z+1/2$; (viii) x, $-y+1/2$, $z-1/2$; (ix) $-x+1$, $y-1/2$, $-z+1/2$.